6 SCIENTIFIC HIGHLIGHT OF THE MONTH: "Density functional theory for superconductors"

Density functional theory for superconductors

M. Lüders[1], M. A. L. Marques[2], A. Floris[3,4], G. Profeta[4], N. N. Lathiotakis[3], C. Franchini[4], A. Sanna[4], A. Continenza[5], S. Massidda[4], E. K. U. Gross[3]

[1]*Daresbury Laboratory, Warrington WA4 4AD, United Kingdom*

[2]*Departamento de Física da Universidade de Coimbra, Rua Larga, 3004-516 Coimbra, Portugal*

[3]*Institut für Theoretische Physik, Freie Universität Berlin, Arnimallee 14, D-14195 Berlin, Germany*

[4]*INFM SLACS, Sardinian Laboratory for Computational Materials Science and Dipartimento di Scienze Fisiche, Università degli Studi di Cagliari, S.P. Monserrato-Sestu km 0.700, I–09124 Monserrato (Cagliari), Italy*

[5]*C.A.S.T.I. - Istituto Nazionale Fisica della Materia (INFM) and Dipartimento di Fisica, Università degli studi dell'Aquila, I-67010 Coppito (L'Aquila) Italy*

Abstract

In this highlight we review density functional theory for superconductors. This formally exact theory is a generalisation of normal-state density functional theory, which also includes the superconducting order parameter and the diagonal of the nuclear density matrix as additional densities. We outline the formal framework and the construction of approximate exchange-correlation functionals. Several aspects of the theory are demonstrated by some examples: a first application to simple metals shows that weakly and strongly coupled superconductors are equally well described. Calculations for MgB_2 with its two gap superconductivity demonstrate the capability to go beyond simple BCS superconductivity. Finally the formalism is applied to aluminium, lithium and potassium under high pressure, describing correctly the experimental behaviour of Al and Li, and predicting fcc-K to become superconducting at high pressures.

1 Introduction

More than one century after the discovery of superconductivity, the prediction of critical temperatures from first principles remains one of the grand challenges of modern solid state physics. It

had taken nearly 50 years until Bardeen, Cooper and Schrieffer (BCS) [1] developed their theory of superconductivity, identifying the mechanism of conventional superconductors as a phonon-mediated pairing of electrons and a condensation into the so-called BCS wave function. This theory, however, only allows for the calculation of universal quantities, such as the ratio of the critical temperature and the gap at zero temperature, and not for material specific properties. The first major step beyond this limitation was Eliashberg theory [2–7], based on many-body perturbation theory in the superconducting state. The difference to normal state calculations is that in the superconducting state also expectation values of two electronic creation or two destruction operators remain finite. They give rise to the anomalous Green's functions which, when evaluated for equal times, result in the superconducting order parameter, introduced already in the BCS theory. In principle, Eliashberg theory is a complete theory of the superconducting state, taking proper account of the electron-phonon (e-ph) interaction and the electron-electron repulsion. In practise, however, the Coulomb repulsion is very difficult to treat and is normally included through the pseudopotential μ^*, whose value is typically fitted to obtain the experimental critical temperature of the material. Therefore Eliashberg theory, in its common practical implementation, cannot be considered a truly ab initio theory either.

The standard tool for material specific first principles calculations of normal-state properties, such as the geometrical or magnetic structure, is density functional theory (DFT). This theory is based on the Hohenberg-Kohn (HK) theorem [8] that guarantees that all physical observables of a system, in particular the total energy, are functionals of the ground-state density. The HK theorem was employed by Kohn and Sham [9] to introduce an auxiliary non-interacting system, subject to an effective potential, constructed such that the non-interacting system reproduces the ground-state density of the fully interacting system. To this end, the total energy functional was rewritten in terms of a part corresponding to this non-interacting system and the remainder, the so-called exchange-correlation (xc) energy functional, which includes all our ignorance about the interacting system. Good approximations to this unknown functional, such as the local (spin) density approximation [L(S)DA], are the key to successful applications of DFT. The LSDA and also the generalised gradient approximation (GGA) have so far triggered a broad variety of accurate applications of DFT, ranging from atomic and molecular systems to solids. It can be said that DFT is the main working horse for virtually all computational material science. For reviews of DFT see, for example, Refs. [10–14].

In this highlight we review how density functional theory can be generalised to superconducting systems [15–17], yielding a theory that overcomes the above mentioned problems and has the potential to become a standard tool for the calculation of superconducting properties.

2 Formal framework

Before turning to the problem of superconductivity, it is instructive to reconsider how magnetic systems are usually treated. The HK theorem states that all observables, in particular also the magnetisation, are functionals of the electronic density *alone*. This, however, assumes the knowledge of the magnetisation as a functional of the density. To approximate this functional is extremely hard and, in practise, one chooses a different approach. The task can be vastly

simplified by treating the magnetisation density $\mathbf{m}(\mathbf{r})$, i.e., the order parameter of the magnetic state, as an additional fundamental density in the density functional framework. An auxiliary field – here a magnetic field $\mathbf{B}_{\rm ext}(\mathbf{r})$ – is introduced, which couples to $\mathbf{m}(\mathbf{r})$ and breaks the corresponding (rotational) symmetry of the Hamiltonian. In other words, it drives the system into the ordered state. The resulting magnetisation then leads to a finite value of the effective magnetic field. If the system wants to be magnetic, the order parameter will survive even if the auxiliary perturbation is switched off again. In this way, the ground-state magnetisation density is determined by minimising the total energy functional (free energy functional for finite temperature calculations) with respect to both the normal density and the magnetisation density. Much simpler approximations to the xc functional (now a functional of two densities) can lead to satisfactory results. This idea forms the basis of the local spin density approximation and, likewise, of current density functional theory [18, 19].

The same idea is also at the heart of density functional theory for superconductors, as formulated by Oliveira, Gross and Kohn [15]. Here the order parameter is the so-called anomalous density,

$$\chi(\mathbf{r},\mathbf{r}') = \langle \hat{\Psi}_\uparrow(\mathbf{r})\hat{\Psi}_\downarrow(\mathbf{r}')\rangle\,, \tag{1}$$

and the corresponding potential is the non-local pairing potential $\Delta(\mathbf{r},\mathbf{r}')$. It can be interpreted as an external pairing field, induced by an adjacent superconductor via the proximity effect. Again, this external field only acts to break the symmetry (here the gauge symmetry) of the system, and is set to zero at the end of the calculation. As in the case of magnetism, the order parameter will be sustained by the self-consistent effective pairing field, if the system wants to be superconducting. The formalism outlined so far captures, in principle, all electronic degrees of freedom. To describe conventional, phonon-mediated, superconductors, also the electron-phonon interaction has to be taken into account. In the weak coupling limit, this phonon-mediated interaction can be added as an additional BCS-type interaction. However, in order to treat also strong electron-phonon coupling, the electronic and the nuclear degrees of freedom have to be treated on equal footing. This can be achieved by a multi-component DFT, based on both the electronic density and the nuclear density [20]. The starting point is the full electron-ion Hamiltonian

$$\hat{H} = \hat{T}^{\rm e} + \hat{U}^{\rm ee} + \hat{T}^{\rm n} + \hat{U}^{\rm nn} + \hat{U}^{\rm en}\,, \tag{2}$$

where $\hat{T}^{\rm e}$ represents the electronic kinetic energy, $\hat{U}^{\rm ee}$ the electron-electron interaction, $\hat{T}^{\rm n}$ the nuclear kinetic energy, and $\hat{U}^{\rm nn}$ the Coulomb repulsion between the nuclei. The interaction between the electrons and the nuclei is described by the term

$$\hat{U}^{\rm en} = -\sum_\sigma \int {\rm d}^3r \int {\rm d}^3R\, \hat{\Psi}^\dagger_\sigma(\mathbf{r})\hat{\Phi}^\dagger(\mathbf{R})\frac{Z}{|\mathbf{r}-\mathbf{R}|}\hat{\Phi}(\mathbf{R})\hat{\Psi}_\sigma(\mathbf{r})\,, \tag{3}$$

where $\hat{\Psi}_\sigma(\mathbf{r})$ and $\hat{\Phi}(\mathbf{R})$ are respectively electron and nuclear field operators. (For simplicity we assume the nuclei to be identical, and we neglect the nuclear spin degrees of freedom. The extension of this framework to a more general case is straightforward.) Note that there is no external potential in the Hamiltonian. In addition to the normal and anomalous electronic densities, we also include the diagonal of the nuclear density matrix [1]

$$\Gamma(\underline{\mathbf{R}}) = \langle \hat{\Phi}^\dagger(\mathbf{R}_1)\ldots\hat{\Phi}^\dagger(\mathbf{R}_N)\hat{\Phi}(\mathbf{R}_N)\ldots\hat{\Phi}(\mathbf{R}_1)\rangle \tag{4}$$

[1] Taking only the nuclear density would lead to a system of strictly non-interacting nuclei which obviously would give rise to non-dispersive, hence unrealistic, phonons.

In order to formulate a Hohenberg-Kohn theorem for this system, we introduce a set of three potentials, which couple to the three densities described above. Since the electron-nuclear interaction, which in normal DFT constitutes the external potential, is treated explicitly in this formalism, it is *not* part of the external potential. The nuclear Coulomb interaction $\hat{U}^{\mathrm{nn}}$ already has the form of an external many-body potential, coupling to $\Gamma(\underline{\mathbf{R}})$, and for the sake of the Hohenberg-Kohn theorem, this potential will be allowed to take the form of an arbitrary N-body potential. All three external potentials are merely mathematical devices, required to formulate a Hohenberg-Kohn theorem. At the end of the derivation they will be set to zero (in case of the external electronic and pairing potentials) and to the nuclear Coulomb interaction (for the external nuclear many-body potential).

As usual, the Hohenberg-Kohn theorem guarantees a one-to-one mapping between the set of the densities $\{n(\mathbf{r}), \chi(\mathbf{r},\mathbf{r}'), \Gamma(\underline{\mathbf{R}})\}$ in thermal equilibrium and the set of their conjugate potentials $\{v^{\mathrm{e}}_{\mathrm{ext}}(\mathbf{r}) - \mu, \Delta_{\mathrm{ext}}(\mathbf{r},\mathbf{r}'), v^{\mathrm{n}}_{\mathrm{ext}}(\underline{\mathbf{R}})\}$. As a consequence, all the observables are functionals of the set of densities. Finally, it assures that the grand canonical potential,

$$\Omega[n,\chi,\Gamma] = F[n,\chi,\Gamma] + \int \mathrm{d}^3 r\, n(\mathbf{r})[v^{\mathrm{e}}_{\mathrm{ext}}(\mathbf{r}) - \mu] \\ - \int \mathrm{d}^3 r \int \mathrm{d}^3 r'\, \left[\chi(\mathbf{r},\mathbf{r}')\Delta^*_{\mathrm{ext}}(\mathbf{r},\mathbf{r}') + \mathrm{h.c.}\right] + \int \mathrm{d}^3 \underline{R}\, \Gamma(\underline{\mathbf{R}}) v^{\mathrm{n}}_{\mathrm{ext}}(\underline{\mathbf{R}})\,, \quad (5)$$

is minimised by the equilibrium densities. We use the notation $A[f]$ to denote that A is a functional of f. The functional $F[n,\chi,\Gamma]$ is universal, in the sense that it does not depend on the external potentials, and is defined by

$$F[n,\chi,\Gamma] = T^{\mathrm{e}}[n,\chi,\Gamma] + T^{\mathrm{n}}[n,\chi,\Gamma] + U^{\mathrm{en}}[n,\chi,\Gamma] + U^{\mathrm{ee}}[n,\chi,\Gamma] - \frac{1}{\beta} S[n,\chi,\Gamma]\,, \quad (6)$$

where S is the entropy of the system,

$$S[n,\chi,\Gamma] = -\mathrm{Tr}\{\hat{\rho}_0[n,\chi,\Gamma]\ln(\hat{\rho}_0[n,\chi,\Gamma])\}\,. \quad (7)$$

The proof of the theorem follows closely the proof of the Hohenberg-Kohn theorem at finite temperatures [21].

3 Kohn-Sham system

In standard DFT one normally defines a Kohn-Sham system, i.e., a non-interacting system chosen such that it has the same ground-state density as the interacting one. In our formalism, the Kohn-Sham system consists of non-interacting (superconducting) electrons, and *interacting* nuclei. It is described by the thermodynamic potential [cf. Eq. (5)]

$$\Omega_{\mathrm{s}}[n,\chi,\Gamma] = F_{\mathrm{s}}[n,\chi,\Gamma] + \int \mathrm{d}^3 r\, n(\mathbf{r})[v^{\mathrm{e}}_{\mathrm{s}}(\mathbf{r}) - \mu_{\mathrm{s}}] \\ - \int \mathrm{d}^3 r \int \mathrm{d}^3 r'\, \left[\chi(\mathbf{r},\mathbf{r}')\Delta^*_{\mathrm{s}}(\mathbf{r},\mathbf{r}') + h.c.\right] + \int \mathrm{d}^3 \underline{R}\, \Gamma(\underline{\mathbf{R}}) v^{\mathrm{n}}_{\mathrm{s}}(\underline{\mathbf{R}})\,, \quad (8)$$

where F_{s} if the counterpart of (6) for the Kohn-Sham system, i.e.,

$$F_{\mathrm{s}}[n,\chi,\Gamma] = T^{\mathrm{e}}_{\mathrm{s}}[n,\chi,\Gamma] + T^{\mathrm{n}}_{\mathrm{s}}[n,\chi,\Gamma] - \frac{1}{\beta} S_{\mathrm{s}}[n,\chi,\Gamma]\,. \quad (9)$$

Here $T_{\rm s}^{\rm e}[n,\chi,\Gamma]$, $T_{\rm s}^{\rm n}[n,\chi,\Gamma]$, and $S_{\rm s}[n,\chi,\Gamma]$ are the electronic and nuclear kinetic energies and the entropy of the Kohn-Sham system, respectively. From Eq. (8) it is clear that the Kohn-Sham nuclei interact with each other through the N-body potential $v_{\rm s}^{\rm n}(\underline{\mathbf{R}})$, while they do not interact with the electrons.

The Kohn-Sham potentials, which are derived in analogy to normal DFT, include the external fields, Hartree, and exchange-correlation terms. The latter account for all many-body effects of the electron-electron and electron-nuclear interactions and are, as usual, given by the respective functional derivatives of the xc energy functional defined through

$$F[n,\chi,\Gamma] = F_{\rm s}[n,\chi,\Gamma] + F_{\rm xc}[n,\chi,\Gamma] + E_{\rm H}^{\rm ee}[n,\chi] + E_{\rm H}^{\rm en}[n,\Gamma]\,. \tag{10}$$

There are two contributions to $E_{\rm H}^{\rm ee}$, one originating from the electronic Hartree potential, and the other from the anomalous Hartree potential

$$E_{\rm H}^{\rm ee}[n,\chi] = \frac{1}{2}\int {\rm d}^3r \int {\rm d}^3r'\,\frac{n(\mathbf{r})n(\mathbf{r}')}{|\mathbf{r}-\mathbf{r}'|} + \int {\rm d}^3r \int {\rm d}^3r'\,\frac{|\chi(\mathbf{r},\mathbf{r}')|^2}{|\mathbf{r}-\mathbf{r}'|}\,. \tag{11}$$

Finally, $E_{\rm H}^{\rm en}$ denotes the electron-nuclear Hartree energy

$$E_{\rm H}^{\rm en}[n,\Gamma] = -Z\sum_\alpha \int {\rm d}^3r \int {\rm d}^3\underline{R}\,\frac{n(\mathbf{r})\Gamma(\underline{\mathbf{R}})}{|\mathbf{r}-\mathbf{R}_\alpha|}\,. \tag{12}$$

The problem of minimising the Kohn-Sham grand canonical potential (8) can be transformed into a set of three differential equations that have to be solved self-consistently: One equation for the nuclei, which resembles the familiar nuclear Born-Oppenheimer equation, and two coupled equations which describe the electronic degrees of freedom and have the algebraic structure of the Bogoliubov-de Gennes [22] equations.

The Kohn-Sham equation for the nuclei has the form

$$\left[-\sum_\alpha \frac{\nabla_\alpha^2}{2M} + v_{\rm s}^{\rm n}(\underline{\mathbf{R}})\right]\Phi_l(\underline{\mathbf{R}}) = \mathcal{E}_l\Phi_l(\underline{\mathbf{R}})\,. \tag{13}$$

We emphasise that the Kohn-Sham equation (13) does not rely on any approximation and is, in principle, exact. In practise, however, the unknown effective potential for the nuclei is approximated by the Born-Oppenheimer surface. As already mentioned, we are interested in solids at relatively low temperature, where the nuclei perform small amplitude oscillations around their equilibrium positions. In this case, we can expand $v_{\rm s}^{\rm n}[n,\chi,\Gamma]$ in a Taylor series around the equilibrium positions, and transform the nuclear degrees of freedom into collective (phonon) coordinates. In harmonic order, the nuclear Kohn-Sham Hamiltonian then reads

$$\hat{H}_{\rm s}^{\rm ph} = \sum_{\lambda,\mathbf{q}} \Omega_{\lambda,\mathbf{q}}\left[\hat{b}_{\lambda,\mathbf{q}}^\dagger \hat{b}\dagger_{\lambda,\mathbf{q}} + \frac{1}{2}\right]\,, \tag{14}$$

where $\Omega_{\lambda,\mathbf{q}}$ are the phonon eigenfrequencies, and $\hat{b}_{\lambda,\mathbf{q}}^\dagger$ creates a phonon of branch λ and wave-vector $\mathbf{q}$. Note that the phonon eigenfrequencies are functionals of the set of densities $\{n,\chi,\Gamma\}$, and can therefore be affected by the superconducting order parameter.

The Kohn-Sham Bogoliubov-de Gennes (KS-BdG) equations read

$$\left[-\frac{\nabla^2}{2}+v_{\rm s}^{\rm e}(\mathbf{r})-\mu\right]u_{n\mathbf{k}}(\mathbf{r})+\int \mathrm{d}^3r'\,\Delta_{\rm s}(\mathbf{r},\mathbf{r}')v_{n\mathbf{k}}(\mathbf{r}')=\tilde{E}_{n\mathbf{k}}\,u_{n\mathbf{k}}(\mathbf{r})\,, \tag{15a}$$

$$-\left[-\frac{\nabla^2}{2}+v_{\rm s}^{\rm e}(\mathbf{r})-\mu\right]v_{n\mathbf{k}}(\mathbf{r})+\int \mathrm{d}^3r'\,\Delta_{\rm s}^*(\mathbf{r},\mathbf{r}')u_{n\mathbf{k}}(\mathbf{r}')=\tilde{E}_{n\mathbf{k}}\,v_{n\mathbf{k}}(\mathbf{r})\,, \tag{15b}$$

where $u_{n\mathbf{k}}(\mathbf{r})$ and $v_{n\mathbf{k}}(\mathbf{r})$ are the particle and hole amplitudes. This equation is very similar to the Kohn-Sham equations in the OGK formalism [15]. However, in the present formulation the lattice potential is not considered an external potential but enters via the electron-ion Hartree term. Furthermore, our exchange-correlation potentials depend on the nuclear density matrix, and therefore on the phonons. Although equations (13) and (15) have the structure of static mean-field equations, they contain, in principle, all correlation and retardation effects through the exchange-correlation potentials.

These KS-BdG equations can be simplified by the so-called decoupling approximation [16, 23], which corresponds to the following ansatz for the particle and hole amplitudes:

$$u_{n\mathbf{k}}(\mathbf{r})\approx u_{n\mathbf{k}}\varphi_{n\mathbf{k}}(\mathbf{r})\,;\quad v_{n\mathbf{k}}(\mathbf{r})\approx v_{n\mathbf{k}}\varphi_{n\mathbf{k}}(\mathbf{r})\,, \tag{16}$$

where the wave functions $\varphi_{n\mathbf{k}}(\mathbf{r})$ are the solutions of the normal Schrödinger equation. In this way the eigenvalues in Eq. (15) become $\tilde{E}_{n\mathbf{k}}=\pm E_{n\mathbf{k}}$, where

$$E_{n\mathbf{k}}=\sqrt{\xi_{n\mathbf{k}}^2+|\Delta_{n\mathbf{k}}|^2}\,, \tag{17}$$

and $\xi_{n\mathbf{k}}=\epsilon_{n\mathbf{k}}-\mu$. This form of the eigenenergies allows us to interpret the pair potential $\Delta_{n\mathbf{k}}$ as the gap function of the superconductor. Furthermore, the coefficients $u_{n\mathbf{k}}$ and $v_{n\mathbf{k}}$ are given by simple expressions within this approximation

$$u_{n\mathbf{k}}=\frac{1}{\sqrt{2}}\mathrm{sgn}(\tilde{E}_{n\mathbf{k}})\mathrm{e}^{\mathrm{i}\phi_{n\mathbf{k}}}\sqrt{1+\frac{\xi_{n\mathbf{k}}}{\tilde{E}_{n\mathbf{k}}}}\,, \tag{18a}$$

$$v_{n\mathbf{k}}=\frac{1}{\sqrt{2}}\sqrt{1-\frac{\xi_{n\mathbf{k}}}{\tilde{E}_{n\mathbf{k}}}}\,. \tag{18b}$$

Finally, the matrix elements $\Delta_{n\mathbf{k}}$ are defined as

$$\Delta_{n\mathbf{k}}=\int \mathrm{d}^3r\int \mathrm{d}^3r'\,\varphi_{n\mathbf{k}}^*(\mathbf{r})\Delta_{\rm s}(\mathbf{r},\mathbf{r}')\varphi_{n\mathbf{k}}(\mathbf{r}')\,, \tag{19}$$

and $\phi_{n\mathbf{k}}$ is the phase $\mathrm{e}^{\mathrm{i}\phi_{n\mathbf{k}}}=\Delta_{n\mathbf{k}}/|\Delta_{n\mathbf{k}}|$. The normal and the anomalous densities can then be easily obtained from:

$$n(\mathbf{r})=\sum_{n\mathbf{k}}\left[1-\frac{\xi_{n\mathbf{k}}}{E_{n\mathbf{k}}}\tanh\left(\frac{\beta}{2}E_{n\mathbf{k}}\right)\right]|\varphi_{n\mathbf{k}}(\mathbf{r})|^2 \tag{20a}$$

$$\chi(\mathbf{r},\mathbf{r}')=\frac{1}{2}\sum_{n\mathbf{k}}\frac{\Delta_{n\mathbf{k}}}{E_{n\mathbf{k}}}\tanh\left(\frac{\beta}{2}E_{n\mathbf{k}}\right)\varphi_{n\mathbf{k}}(\mathbf{r})\varphi_{n\mathbf{k}}^*(\mathbf{r}')\,. \tag{20b}$$

Within the decoupling approximation outlined above, a major part of the calculation is to self-consistently determine the effective pairing potential. As will be seen in the next sections, the actual approximations for the xc functionals are not explicit functionals of the densities, but

rather functionals of the potentials, still being implicit functionals of the density. Therefore the task of calculating the effective pair potential is to solve the non-linear functional equation

$$\Delta_{\mathrm{s},n\mathbf{k}} = \Delta_{\mathrm{xc},n\mathbf{k}}[\mu, \Delta_\mathrm{s}]. \tag{21}$$

In the vicinity of the critical temperature, where the order parameter and hence the pairing potential vanishes, this equation can be linearised, giving rise to a BCS-like gap equation:

$$\breve{\Delta}_{n\mathbf{k}} = -\frac{1}{2}\sum_{n'\mathbf{k}'} \mathcal{F}_{\mathrm{Hxc}\; n\mathbf{k},n'\mathbf{k}'}[\mu] \frac{\tanh\left(\frac{\beta}{2}\xi_{n'\mathbf{k}'}\right)}{\xi_{n'\mathbf{k}'}} \breve{\Delta}_{n'\mathbf{k}'}\,, \tag{22}$$

where the anomalous Hartree exchange-correlation kernel of the homogeneous integral equation reads

$$\mathcal{F}_{\mathrm{Hxc}\; n\mathbf{k},n'\mathbf{k}'}[\mu] = -\left.\frac{\delta\Delta_{\mathrm{Hxc}\, n\mathbf{k}}}{\delta\chi_{n'\mathbf{k}'}}\right|_{\chi=0} = \left.\frac{\delta^2(E^{\mathrm{ee}}_{\mathrm{H}} + F_{\mathrm{xc}})}{\delta\chi^*_{n\mathbf{k}}\delta\chi_{n'\mathbf{k}'}}\right|_{\chi=0}. \tag{23}$$

Although this linearised gap equation is strictly valid only in the vicinity of the transition temperature, we use the same kernel $\mathcal{F}_{\mathrm{Hxc}}$ in a partially linearised equation, that has the same structure but contains the energies $E_{n\mathbf{k}}$ in place of the $\xi_{n\mathbf{k}}$, also at lower temperatures. Furthermore, we split the kernel into a purely diagonal part $\mathcal{Z}$ and a truly off-diagonal part $\mathcal{K}$,

$$\Delta_{n\mathbf{k}} = -\mathcal{Z}_{n\mathbf{k}}\Delta_{n\mathbf{k}} - \frac{1}{2}\sum_{n'\mathbf{k}'} \mathcal{K}_{n\mathbf{k},n'\mathbf{k}'} \frac{\tanh\left(\frac{\beta}{2}E_{n'\mathbf{k}'}\right)}{E_{n'\mathbf{k}'}} \Delta_{n'\mathbf{k}'}\,. \tag{24}$$

Explicit expressions for $\mathcal{Z}_{n\mathbf{k}}$ and $\mathcal{K}_{n\mathbf{k},n'\mathbf{k}'}$ will be given below.

4 Functionals

So far, only the formal framework of the theory was presented. But, like for any DFT, its success strongly depends on the availability of reliable approximations to the xc functional. For normal-state calculations, a variety of such functionals is available, ranging from the local density approximation (LDA), based on highly accurate Quantum Monte Carlo calculations of the homogeneous electron gas, and generalised gradient approximations (GGA), to orbital functionals such as exact exchange, and combinations thereof.

Recently, some first approximations to the xc energy functional for superconductors have been presented. In contrast to the normal-state functionals, here the functional also depends on the anomalous density. Furthermore, in order to describe conventional superconductors, it must contain the electron-phonon interaction, as well as the electronic Coulomb correlations.

The proposed functional is based on many-body perturbation theory in the superconducting state, and is guided by parallels to the Eliashberg theory. The building blocks of many-body perturbation theory are the electronic propagators (including the so-called anomalous propagators in the superconducting state), the phonon propagator and the electron-electron as well as the electron-phonon interaction. It can be seen from quite general arguments that all diagrams can be classified into purely electronic ones and diagrams including the phonon propagator. This classification warrants that these two contributions can be treated in a different way, because they describe different mechanisms.

For the electronic terms, we construct a local density approximation, in other words, we approximate the xc energy density of a homogeneous but superconducting electron gas [24]. Since the anomalous density is a non-local quantity, the xc energy remains a functional – rather than a function – even in the homogeneous electron gas. This, unfortunately, makes the construction of approximations much more complicated, and, at present, rules out full fledged Quantum Monte Carlo calculations, as available for the normal state. Instead, functionals based on the RPA [24] and its static limit [17] have been proposed. The latter is quite easy to implement and was used (with slight variations, described in Ref. [17]) for the calculations presented below.

For the electron-phonon contributions an LDA-type functional is not meaningful, because the homogeneous electron gas does not posses phonons. Instead, the e-ph contribution to the xc energy is directly calculated from many-body perturbation theory by evaluating the two lowest order diagrams, shown in Figure 1. The expressions for the xc energies can be found in Ref. [16].

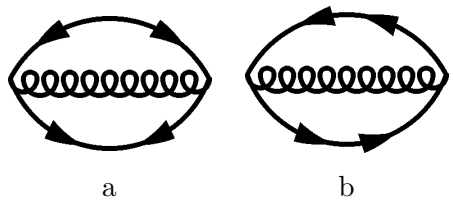

Figure 1: Lowest order phononic (a, b) contributions to $F_{\rm xc}$. The two types of electron propagators correspond to the normal and anomalous Green's functions.

Besides the Coulomb repulsion and the electron-phonon coupling, spin-fluctuations constitute another important mechanism. Ferromagnetic spin-fluctuations are known to lower the critical temperature in materials such as vanadium and even to suppress superconductivity in palladium, while antiferromagnetic spin-fluctuations are amongst the candidates for the mechanism of the high-T_c superconductors. Spin fluctuations can be treated in a similar way to the electron-phonon term by replacing the phonon-propagator in the diagrams by the spin-fluctuation propagator. This has been proposed in the context of the Eliashberg theory [25, 26] and recently a first approximation in the context of DFT for superconductors was constructed [27].

5 Potentials and kernels

The functionals described above are only implicit functionals of the densities. The desired functional derivatives can nevertheless be evaluated by applying the chain rule of functional derivatives, similar to the procedure used in the optimised effective potential method [28, 29]. The xc energy is an explicit functional of the pairing potential and the chemical potential, and therefore we can write

$$\Delta_{{\rm xc}\,n\mathbf{k}} = -\frac{\delta F_{\rm xc}}{\delta\mu}\frac{\delta\mu}{\delta\chi^*_{n\mathbf{k}}} - \sum_{n'\mathbf{k}'}\left[\frac{\delta F_{\rm xc}}{\delta|\Delta_{n'\mathbf{k}'}|^2}\frac{\delta|\Delta_{n'\mathbf{k}'}|^2}{\delta\chi^*_{n\mathbf{k}}} + \frac{\delta F_{\rm xc}}{\delta(\phi_{n'\mathbf{k}'})}\frac{\delta(\phi_{n'\mathbf{k}'})}{\delta\chi^*_{n\mathbf{k}}}\right] . \tag{25}$$

The partial derivatives of $F_{\rm xc}$ can be calculated directly. The remaining functional derivatives are somewhat harder to obtain, but can be derived from the definitions of the densities, Eqs. (20),

Table 1: Critical temperature (left panel) and superconducting gap at Fermi level and $T = 0.01\,\mathrm{K}$ (right panel), compared with experiment [30]. We also show the total electron-phonon coupling constant λ [31, 32]. While TF-ME represents an approximation with the full matrix elements, TF-SK and TF-FE correspond to simplified expressions. For details see Ref. [17].

	T_c [K]						Δ_0 [meV]				
	TF-ME	TF-SK	TF-FE	exp	λ		TF-ME	TF-SK	TF-FE	exp	λ
Mo	—	0.33	0.54	0.92	0.42	Mo	—	0.049	0.099	—-	0.42
Al	0.90	0.90	1.0	1.18	0.44	Al	0.14	0.15	0.15	0.179	0.44
Ta	3.7	2.7	4.8	4.48	0.84	Ta	0.63	0.53	0.76	0.694	0.84
Pb	6.9	7.2	6.8	7.2	1.62	Pb	1.34	1.40	1.31	1.33	1.62
Nb	9.5	8.4	9.4	9.3	1.18	Nb	1.74	1.54	1.79	1.55	1.18

and from the fact that the particle density and the anomalous density are independent variables, leading to the condition

$$\frac{\delta n(\mathbf{x})}{\delta \chi^*(\mathbf{r}, \mathbf{r}')} = 0\,. \tag{26}$$

After a number of further approximations (see [16, 17]), the final expressions for the functionals $\mathcal{Z}_{n\mathbf{k}}$ and $\mathcal{K}_{n\mathbf{k},n'\mathbf{k}'}$ in the gap equation (24) read as follows. There are two contributions stemming from the electron-phonon interaction: i) The non-diagonal one is:

$$\mathcal{K}^{\mathrm{ph}}_{n\mathbf{k},n'\mathbf{k}'} = \frac{2}{\tanh\left(\frac{\beta}{2}\xi_{n\mathbf{k}}\right)\tanh\left(\frac{\beta}{2}\xi_{n'\mathbf{k}'}\right)} \times \sum_{\lambda,\mathbf{q}} \left| g^{n\mathbf{k},n'\mathbf{k}'}_{\lambda,\mathbf{q}} \right|^2 \left[I(\xi_{n\mathbf{k}}, \xi_{n'\mathbf{k}'}, \Omega_{\lambda,\mathbf{q}}) - I(\xi_{n\mathbf{k}}, -\xi_{n'\mathbf{k}'}, \Omega_{\lambda,\mathbf{q}}) \right], \tag{27}$$

where $g^{n\mathbf{k},n'\mathbf{k}'}_{\lambda,\mathbf{q}}$ are the electron-phonon coupling constants and the function I is defined as

$$I(\xi, \xi', \Omega) = f_\beta(\xi)\, f_\beta(\xi')\, n_\beta(\Omega) \left[\frac{\mathrm{e}^{\beta\xi} - \mathrm{e}^{\beta(\xi'+\Omega)}}{\xi - \xi' - \Omega} - \frac{\mathrm{e}^{\beta\xi'} - \mathrm{e}^{\beta(\xi+\Omega)}}{\xi - \xi' + \Omega} \right]. \tag{28}$$

In the previous expression f_β and n_β are the Fermi-Dirac and Bose-Einstein distributions; ii) The second contribution is diagonal in $n\mathbf{k}$ and reads

$$\mathcal{Z}^{\mathrm{ph}}_{n\mathbf{k}} = \frac{1}{\tanh\left(\frac{\beta}{2}\xi_{n\mathbf{k}}\right)} \sum_{n'\mathbf{k}'} \sum_{\lambda,\mathbf{q}} \left| g^{n\mathbf{k},n'\mathbf{k}'}_{\lambda,\mathbf{q}} \right|^2 \left[J(\xi_{n\mathbf{k}}, \xi_{n'\mathbf{k}'}, \Omega_{\lambda,\mathbf{q}}) + J(\xi_{n\mathbf{k}}, -\xi_{n'\mathbf{k}'}, \Omega_{\lambda,\mathbf{q}}) \right], \tag{29}$$

where the function J is defined by

$$J(\xi, \xi', \Omega) = \tilde{J}(\xi, \xi', \Omega) - \tilde{J}(\xi, \xi', -\Omega)\,, \tag{30}$$

and we have

$$\tilde{J}(\xi, \xi', \Omega) = -\frac{f_\beta(\xi) + n_\beta(\Omega)}{\xi - \xi' - \Omega} \left[\frac{f_\beta(\xi') - f_\beta(\xi - \Omega)}{\xi - \xi' - \Omega} - \beta f_\beta(\xi - \Omega) f_\beta(-\xi' + \Omega) \right]. \tag{31}$$

On the other hand, the Coulomb interaction leads to the term

$$\mathcal{K}^{\text{TF-ME}}_{n\mathbf{k},n'\mathbf{k}'} = v^{\mathrm{TF}}_{n\mathbf{k},n'\mathbf{k}'}\,, \tag{32}$$

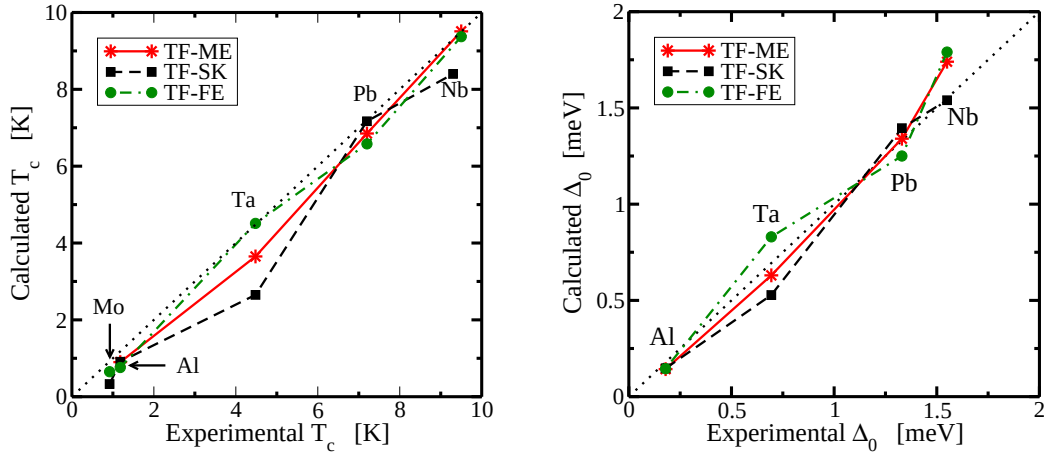

Figure 2: The critical temperature and superconducting gap at Fermi level and $T = 0.01\,\mathrm{K}$, compared with experiment. The numerical values can be found in Table 1.

with the definition

$$v^{\mathrm{TF}}_{n\mathbf{k},n'\mathbf{k}'} = \int \mathrm{d}^3 r \int \mathrm{d}^3 r'\, v^{\mathrm{TF}}(\mathbf{r}-\mathbf{r}')\varphi^*_{n\mathbf{k}}(\mathbf{r})\varphi_{n\mathbf{k}}(\mathbf{r}')\varphi_{n'\mathbf{k}'}(\mathbf{r})\varphi^*_{n'\mathbf{k}'}(\mathbf{r}') \tag{33}$$

and

$$v^{\mathrm{TF}}(\mathbf{r}-\mathbf{r}') = \frac{e^{-k_{\mathrm{TF}}|\mathbf{r}-\mathbf{r}'|}}{|\mathbf{r}-\mathbf{r}'|}\,, \tag{34}$$

with the Thomas-Fermi screening length, $k^2_{\mathrm{TF}} = 4\pi N(0)$. Finally, $N(0)$ denotes the total density of states at the Fermi level.

It should be noted here that these approximations, such as the partial linearisation, are used for all systems studied below, and hence the constructed exchange and correlation functionals remain truly universal.

6 Results

In order to assess the accuracy of the method and the functionals described above, we calculated the gaps and transition temperatures for a set of simple metals, including typical weak coupling systems, such as Al and Mo, but also the strong coupling metals Pb and Nb. Table 1 and Fig. 2 summarise the results and compare the theoretical values for the transition temperature and the gap at zero temperature with experimental values. The different theoretical results correspond to slightly different approximations to the electronic part of the xc pairing potential, which are described in reference [17]. The results demonstrate that the method works equally well for the weak coupling superconductors Al and Mo, as well as for intermediate (Ta) and strong coupling superconductors, such as Pb and Nb. It should be noted that we also applied the method to Cu, which does not show superconductivity in experiments, and we were not able to find a non-trivial solution of the gap equation, showing clearly that the theory is reliable.

Figure 3 shows the pair potential Δ_k plotted against the single particle energies $\epsilon_k - \mu$. The plots reveal how the retardation effects work in this formalism. As already pointed out by Morel and

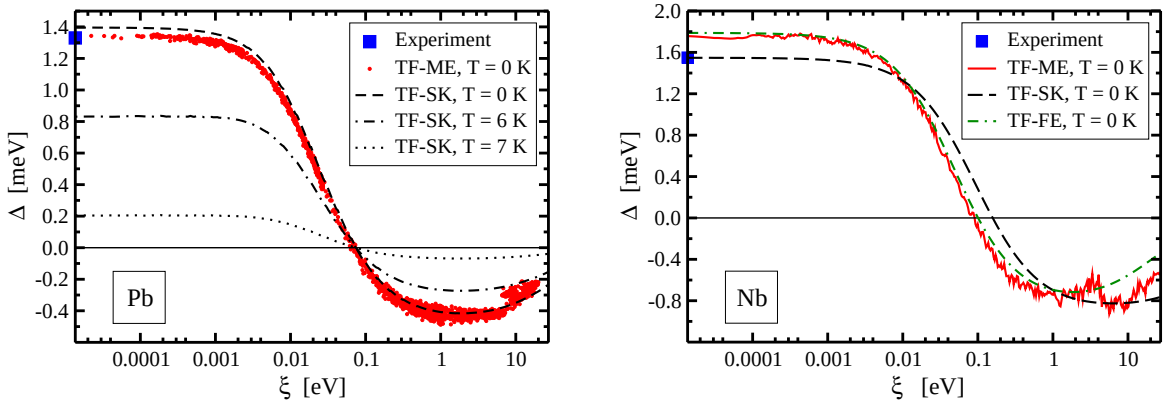

Figure 3: The function $\Delta(\xi_{n\mathbf{k}}, T)$ for lead (left panel) and niobium (right panel).

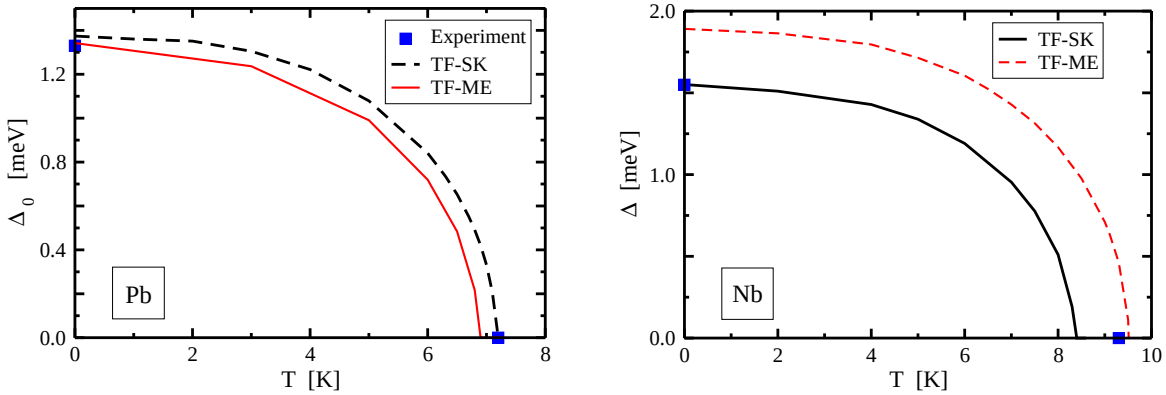

Figure 4: The gap function at the Fermi surface Δ_0 for Pb and Nb as a function of temperature.

Anderson [33], the system can benefit from the repulsive Coulomb interaction by changing sign of the pair potential away from the Fermi surface. In fact, our gap equation does not converge to a superconducting solution unless all electronic states in a large energy window are included. This is also the mechanism which in the Eliashberg theory gives rise to the renormalised Coulomb pseudopotential μ^*. It should be pointed out that no such pseudo-potential was used here. It is the full (screened) Coulomb interaction, that enters the corresponding term of the gap equation. The renormalisation is a result of our calculation. Finally, Figure 4 shows the temperature dependence of the gap.

The very satisfactory results for simple metals gave us confidence to apply the formalism also to non-trivial systems. A material that has raised much interest over the last years is MgB_2. Although the material has been known and well-studied for a long time, its superconductivity with the critical temperature of 39.5 K (the highest among phonon-mediated superconductors) was discovered only recently. Its two-gap nature, observed experimentally, classifies this superconductor as a non-BCS superconductor, which makes it a very interesting and important test case.

The normal state of MgB_2 is characterised by a Fermi-surface with several sheets of different orbital character (see e.g. Ref. [34]). In particular, the tubular structures with σ character are

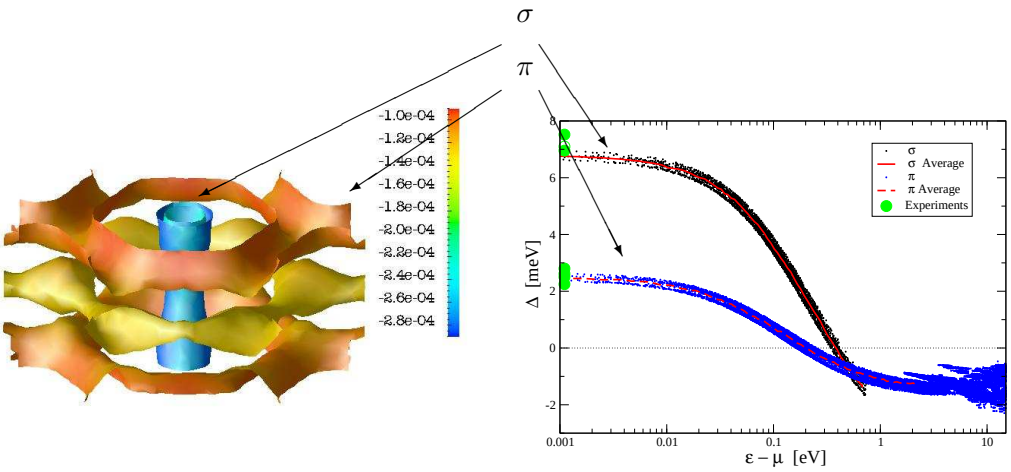

Figure 5: Calculated superconducting gap of MgB_2 as a function of energy ($T = 0\,\mathrm{K}$). The two values correspond to the two sheets of the Fermi-surface, depicted in the left panel.

very strongly coupled to the E_{2g} phonon mode, that corresponds to a B-B bond-stretching in the boron planes [34–36]. MgB_2 also has three-dimensional π bands, that give rise to a complicated Fermi surface. Without holes in the σ bands, the compound would not be superconducting, like AlB_2. The π bands are coupled much less efficiently to phonons, but are nevertheless crucial to superconductivity.

In our density functional calculations we used the four, band resolved, Eliashberg functions, $(\alpha^2 F_{n,n'}(\Omega); n, n' = \sigma, \pi)$, previously employed within a two-band Eliashberg scheme by Golubov *et al.* [37]. Our procedure keeps the fundamental distinction between σ and π gaps, analogously to the Eliashberg calculations reported to date. Further details of the calculation can be found in Ref. [38].

In Fig. 5 we plot the energy gap as a function of (positive) energy distance from the Fermi energy (the gap function exhibits particle-hole symmetry to a good extent). We can see that the two gaps of the material, Δ_σ and Δ_π, arise naturally from our calculations. The σ gap is defined only up to the energy of the top of the σ band. Both Δ_σ and Δ_π are anisotropic. This results from the anisotropy of the Coulomb potential matrix elements – roughly 0.4 meV, $\approx 6\%$ of Δ_σ at the FS – and gets much larger at high energy, where there are many bands with different character. The averages of Δ_σ and Δ_π at the Fermi level (6.8 meV and 2.45 meV respectively) are in excellent agreement with experiment.

In Fig. 6 (panel (**a**)), the superconducting gaps are plotted versus temperature, together with a few experimental results. The agreement is striking: the values of T_c (34.1 K) and of Δ_σ and Δ_π at $T = 0\,\mathrm{K}$ are very close to the experimental data. Moreover, the temperature behaviour of both gaps, along with their strongly non-BCS behaviour, are very well reproduced. Obviously, unlike calculations performed using the Eliashberg theory, we do not reproduce exactly the experimental critical temperature, as our calculations are not fitted to match any experimental quantity.

We also calculated the Kohn-Sham entropy as a function of temperature and, from its temperature derivative, the specific heat. In Fig. 6 (panel (**b**)), we plot our calculated versus the

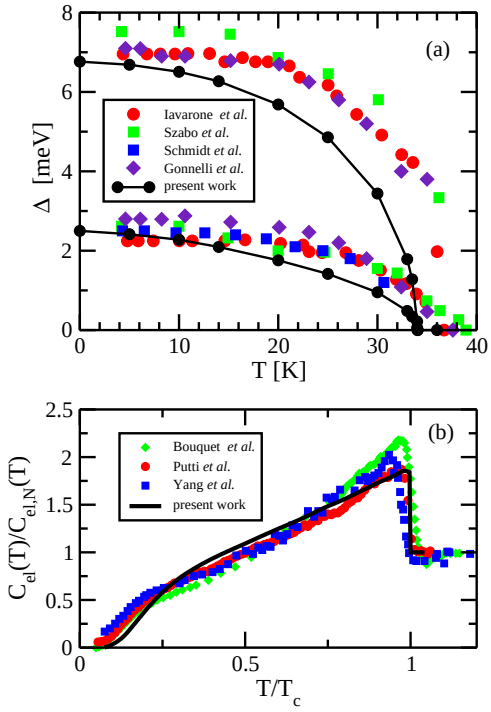

Figure 6: Superconducting gaps at the FS and specific heat of MgB_2. Panel (**a**): Comparison between theoretical and experimental gap at the FS plotted as a function of temperature. The calculated gaps and T_c (34.1 K) are obtained without the use of any adjustable parameter. Panel (**b**): Experimental and calculated electronic specific heat, as a function of T/T_c.

experimental (see Refs. [39–41]) reduced specific heat as a function of temperature, normalised to T_c. For T_c, we used the corresponding calculated and experimental values. Both the shape of the curve as well as the discontinuity at T_c are almost perfectly reproduced by the calculation. We recall that the shoulder of this curve at low temperature comes from the presence of the smaller π gap and that our Δ_σ/Δ_π is slightly different from the experimental ratio.

Another interesting application of the theory is the study of metals under high pressure. Within the class of phonon mediated superconductors, the effect of high pressure has been the subject of many investigations. These studies have revealed new peculiarities such as the strong material dependence of the onset of superconductivity at extreme densities: applied pressure suppresses superconductivity in some materials while favouring it in others [42]. Even for simple metals, the physics underlying pressure effects on the superconducting properties can be very complicated. For example, Li [42–49] and Al [50–52], despite behaving in many respects like nearly free electron gases, exhibit very different behaviours, still only partially understood within Eliashberg theory. At ambient pressure, Al is a superconductor with $T_c = 1.18$ K [50]. Application of hydrostatic pressure rapidly reduces the critical temperature bringing it down to 0.075 K at 6.2 GPa [50]. Li, on the other hand, is a rather complex material, despite the popular belief that it behaves just like a simple metal. Below 77 K and zero pressure, it shows a martensitic transition to energetically competing closed packed structures [53]. From 7.5 to 70 GPa it undergoes several structural transitions [43] which may suggest the presence of strong e-ph interactions. No sign of a transition to a superconducting state was found up to ≈ 20 GPa. However, at higher pressures,

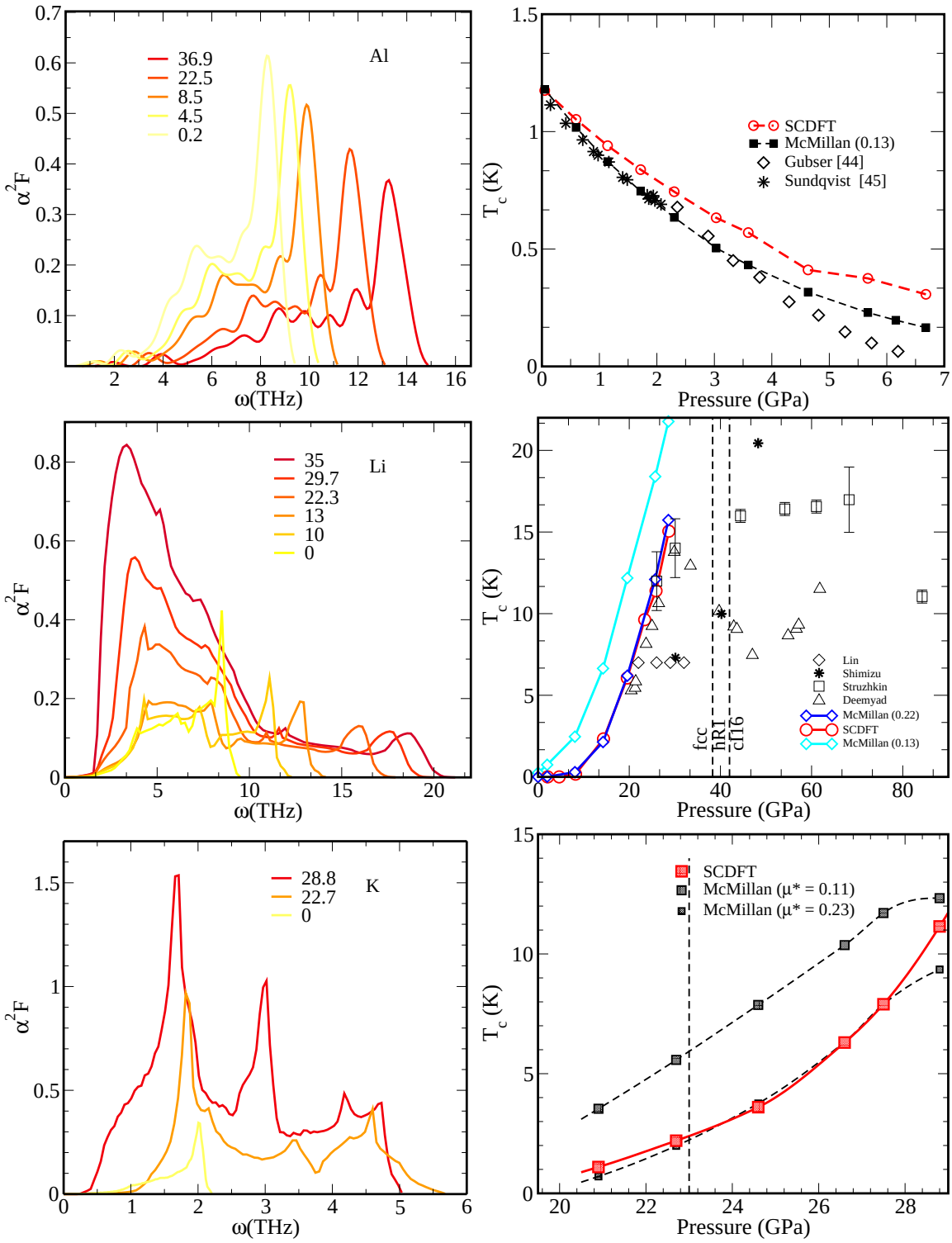

Figure 7: Left Column: Calculated $\alpha^2F(\omega)$ for Al (top), Li (middle) and K (down) at different pressures (inset in each graph). Right column: Calculated and experimental (for Al and Li) T_c for fcc-Al (upper panel), fcc-Li (middle panel) and fcc-K (lower panel) as a function of pressure. Vertical dashed lines indicate the pressure values where structural transitions occur (see text). In the present work only the fcc phase was considered; therefore for Li at pressures larger than $\approx$ 39 GPa, where the fcc phase becomes unstable, our estimates cannot be compared to the experimental values.

Li becomes a superconductor [44–47]. In the range 20-38.3 GPa, where Li crystalizes in an fcc structure, experiments by Shimizu [45], Struzhkin [46], and Deemyad [47] found that T_c increases rapidly with pressure, reaching values around 12–17 K (one of the highest T_c observed so far in any elemental superconductor). However, experiments report different behaviours and quite large deviations.

In Fig. 7 we show the calculated pressure dependence of T_c for Al (upper panel), Li (middle panel), and K (lower panel), compared with experimental results. (Details about the calculations can be found in Refs. [54, 55].) For Al, the calculated zero pressure T_c =1.18 K matches exactly the experimental value.[2] Upon compression, the calculation reproduces quite well the rapid decrease of T_c. A reduction by a factor of 10 with respect to the zero-pressure value is obtained at a pressure ($\simeq$ 8.5 GPa) slightly higher than experiment (6.2 GPa). Similar theoretical results are obtained within the standard McMillan formula [56] (open circles in Fig. 7) using μ^*=0.13 in agreement with previous calculations [52]. The small values of T_c in this pressure range make it quite difficult to extract a good estimate, from both experiments and theory. Nevertheless, the calculations show the asymptotic saturation of T_c rather than the linear decay suggested by experimental data. This discrepancy (with the only experiment available) calls for further experimental investigations in this pressure range.

In the middle panel of Fig. 7 we report the available experiments for Li compared with our calculated values. In the pressure range from 20 to 35 GPa, where the newer experiments [46,47] are in agreement and show a clear increase of T_c with increasing pressure, our calculated results reproduce the experimental trend of T_c and sit close to the experimental values. The calculated pressure which determines the onset of the superconducting state is about 10 GPa, where we predict $T_c \approx 0.2$ K. This finding agrees with Deemyad and Schilling [47], who claim that no superconducting transition above 4 K exists below 20 GPa. Our result is in good agreement with the highest measured T_c, 14 K [47], 16 K [46] and 17 K [45], and improves significantly upon the theoretical estimates by Christensen *et al.* [48], who discussed a paramagnon (i.e., spin fluctuations) dependent T_c varying between 45 and 75 K.

Due to the first principles nature of the method, it is feasible to make predictions on unknown superconductors: we apply the method to find a possible superconducting instability in potassium under pressure. Fcc-K shows a behaviour quite similar to Li: beyond a pressure threshold (20 GPa) T_c rises rapidly. In the range where phonons were found to be stable, it reaches $\sim$ 11 K; the experimentally observed instability of the fcc phase, however, limits this value to $\sim$ 2 K.

We relate the appearance of superconductivity in Li and K to an incipient phase transition, which gives rise to phonon softening and very strong electron-phonon coupling, that then leads to the unusually high transition temperatures. In addition, our calculations for Li and K confirm that a full treatment of electronic and phononic energy scales is required, which is in agreement with previous arguments by Richardson and Ashcroft [57].

The different behaviour of Al on one side and Li and K on the other can be understood by analysing the Eliashberg function as a function of pressure (see Fig. 7). In Al, the phonon

[2] This value is slightly different from the ones reported in Table 1, where the e-ph λ included was taken from Ref. [32]. More details are given in Ref. [54].

frequencies increase as the pressure rises, corresponding to the normal stiffening of phonons with increasing pressure. In addition, the height of the peaks in the Eliashberg spectral function $\alpha^2F(\Omega)$ decreases with increasing pressure. These factors contribute to a decrease of the overall coupling constant λ and, consequently, of the critical temperature T_c.

For alkali metals the situation is completely different: due to the incipient phase transitions, a phonon softening at low frequencies increases the value of λ in both materials. However, the different topology of the Fermi surfaces and the different range of the phonon frequencies sets the critical temperature much higher in lithium with respect to potassium. For more details see Ref. [54, 55]

7 Conclusion

We have developed a truly ab-initio approach to superconductivity without any adjustable parameters. The key feature is that the electron-phonon interaction and the Coulombic electron-electron repulsion are treated on the same footing. This is achieved within a density-functional framework, based on three "densities": the ordinary electronic density, the superconducting order parameter, and the diagonal of the nuclear N-body density matrix. The formalism leads to a set of Kohn-Sham equations for the electrons and the nuclei. The electronic Kohn-Sham equations have the structure of Bogoliubov-de Gennes equations but, in contrast to the latter, they incorporate normal and anomalous xc potentials. Likewise, the Kohn-Sham equation describing the nuclear motion contains, besides the bare nuclear Coulomb repulsion, an exchange-correlation interaction.

The exchange-correlation potentials are functional derivatives of a universal functional $F_{\rm xc}[n, \chi, \Gamma]$ that represents the exchange-correlation part of the free energy. Approximations for this functional were then derived by many-body perturbation theory. To this end, the effective nuclear interaction was expanded to second order in the displacements from the nuclear equilibrium positions. By introducing the usual collective (phonon) coordinates, the nuclear Kohn-Sham equation is then transformed into a set of harmonic oscillator equations describing independent phonons. These non-interacting phonons, together with non-interacting but superconducting (Kohn-Sham) electrons serve as unperturbed system for a Görling-Levy-type perturbative expansion [58] of $F_{\rm xc}$. The electron-phonon interaction and the bare electronic Coulomb repulsion, as well as some residual exchange-correlation potentials, are treated as the perturbation. In this way, both Coulombic and electron-phonon couplings are fully incorporated.

The solution of the KS-Bogoliubov-de Gennes equation (or the KS gap equation together with the normal-state Schrödinger equation) fully determines the Kohn-Sham system. Therefore, within the usual approximation to calculate observables from the Kohn-Sham system, one can apply the full variety of expressions for physical quantities, known from phenomenological Bogoliubov-de Gennes theory, also in the present framework.

Superconducting properties of simple conventional superconductors have been computed without any experimental input. In this way, we were able to test the theory and to assess the quality of the functionals proposed. The most important result is that the calculated transition temperatures and superconducting gaps are in good agreement with experimental values. The

largest deviations from the experimental results are found for the elements in the weak coupling limit with Mo being the most pronounced example. We also calculated the isotope effect for Mo and Pb (see Ref. [17]), achieving again rather good agreement with experiment. These results clearly show that retardation effects are correctly described by the theory.

For MgB_2 we obtained the value of T_c, the two gaps, as well as the specific heat as a function of temperature in very good agreement with experiment. We stress the predictive power of the approach presented: Being, by its very nature, a fully ab-initio approach, it does not require semi-phenomenological parameters, such as μ^*. Nevertheless, it is able to reproduce with good accuracy superconducting properties, previously out of reach of first-principles calculations.

Finally, we also calculated the superconducting transition temperature of Al, K and Li under high pressure from first principles. The results obtained for Al and Li are in very good agreement with experiment, and account for the opposite behaviour of these two metals under pressure. Furthermore, the increase of T_c with pressure in Li is explained in terms of the strong e-ph coupling, which is due to changes in the topology of the Fermi surface, and is responsible for the observed structural instability. Finally, our results for fcc-K provide predictions interesting enough to suggest experimental work on this system.

References

[1] J. Bardeen, L. N. Cooper, and J. R. Schrieffer, Phys. Rev. **108**, 1175 (1957).

[2] G. M. Eliashberg, Sov. Phys. JETP **11**, 696 (1960).

[3] D. J. Scalapino, J. R. Schrieffer, and J. W. Wilkins, Phys. Rev. **148**, 263 (1966).

[4] J. R. Schrieffer, *Theory of Superconductivity*, Vol. 20 of *Frontiers in Physics* (Addison-Wesley, Reading, 1964).

[5] D. J. Scalapino, in *Superconductivity*, edited by R. D. Parks (Marcel Dekker, New York, 1969), Vol. 1, Chap. 10, p. 449.

[6] P. B. Allen and B. Mitrovic, *Solid State Physics*, edited by F. Seitz (Academic Press, Inc., New York, 1982), Vol. 37, p. 1.

[7] J. P. Carbotte, Rev. Mod. Phys. **62**, 1027 (1990).

[8] P. Hohenberg and W. Kohn, Phys. Rev. **136**, B864 (1964).

[9] W. Kohn and L.J. Sham, Phys. Rev. **140**, A1133 (1965).

[10] R.M. Dreizler and E.K.U. Gross, *Density Functional Theory* (Springer, Berlin, 1990).

[11] H. Eschrig, *The Fundamentals of Density Functional Theory*, Vol. 32 of *Teubner-Texte zur Physik* (B. G. Teubner Verlagsgesellschaft, Stuttgart-Leipzig, 1996).

[12] *Density Functional Theory*, Vol. 337 of *NATO ASI Series B*, edited by E.K.U. Gross and R.M. Dreizler (Plenum Press, New York, 1995).

[13] *A Primer in Density Functional Theory*, Vol. 620 of *Lecture Notes in Physics*, edited by C. Fiolhais, F. Nogueira, and M. Marques (Springer, 2003).

[14] R. O. Jones and O. Gunnarsson, Rev. Mod. Phys. **61**, 689 (1989).

[15] L. N. Oliveira, E. K. U. Gross, and W. Kohn, Phys. Rev. Lett. **60**, 2430 (1988).

[16] M. Lüders, M. A. L. Marques, N. N. Lathiotakis, A. Floris, G. Profeta, L. Fast, A. Continenza, S. Massidda, and E. K. U. Gross, Phys. Rev. B **72**, 024545 (2005).

[17] M. A. L. Marques, M. Lüders, N. N. Lathiotakis, G. Profeta, A. Floris, L. Fast, A. Continenza, E. K. U. Gross, and S. Massidda, Phys. Rev. B **72**, 024546 (2005).

[18] G. Vignale and Mark Rasolt, Phys. Rev. Lett. **59**, 2360 (1987).

[19] G. Vignale and Mark Rasolt, Phys. Rev. B **37**, 10685 (1988).

[20] T. Kreibich and E. K. U. Gross, Phys. Rev. Lett. **86**, 2984 (2001).

[21] N. D. Mermin, Phys. Rev. **137**, A1441 (1965).

[22] N. N. Bogoliubov, Sov. Phys. JETP **7**, 41 (1958).

[23] E. K. U. Gross and Stefan Kurth, Int. J. Quantum Chem. Symp. **25**, 289 (1991).

[24] S. Kurth, M. Marques, M. Lüders, and E. K. U. Gross, Phys. Rev. Lett. **83**, 2628 (1999).

[25] H. Rietschel and H. Winter, Phys. Rev. Lett. **43**, 1256 (1979).

[26] R. C. Zehder and H. Winter, J.Phys.: Condens. Matter **2**, 7479 (1990).

[27] M. Wierzbowska, Eur. Phys. J. B **48**, 207 (2005).

[28] T. Grabo, T. Kreibich, S. Kurth, and E. K. U. Gross, in *Strong Coulomb Correlations in Electronic Structure Calculations: Beyond the Local Density Approximation*, edited by V. I. Anisimov (Gordon and Breach, 2000), pp. 203 – 311.

[29] T. Grabo, E.K.U. Gross, and M. Lüders, Orbital Functionals in Density Functional Theory: The Optimized Effective Potential Method, Highlight of the month in Psi-k Newsletter 16, 1996.

[30] N. W. Ashcroft and N. D. Mermin, *Solid State Physics* (Saunders College Publishing, Fort Worth, 1976).

[31] S. Yu. Savrasov, Phys. Rev. Lett. **69**, 2819 (1992).

[32] S. Y. Savrasov and D. Y. Savrasov, Phys. Rev. B **54**, 16487 (1996).

[33] P. Morel and P. W. Anderson, Phys. Rev. **125**, 1263 (1962).

[34] J. Kortus, I. I. Mazin, K. D. Belashchenko, V. P. Antropov, and L. L. Boyer, Phys. Rev. Lett. **86**, 4656 (2001).

[35] J. M. An and W. E. Pickett, Phys. Rev. Lett. **86**, 4366 (2001).

[36] Y. Kong, O. V. Dolgov, O. Jepsen, and O. K. Andersen, Phys. Rev. B **64**, 020501 (2001).

[37] A. A. Golubov, J. Kortus, O. V. Dolgov, O. Jepsen, Y. Kong, O. K. Andersen, B. J. Gibson, K. Ahn, and R. K. Kremer, J. Phys.: Condens. Matter **14**, 1353 (2002).

[38] A. Floris, G. Profeta, N. N. Lathiotakis M. Lüders, M. A. L. Marques, C. Franchini, E. K. U. Gross, A. Continenza, and S. Massidda, Phys. Rev. Lett. **94**, 037004 (2005).

[39] M. Putti, M. Affronte, P. Manfrinetti, and A. Palenzona, Phys. Rev. B **68**, 094514 (2003).

[40] F. Bouquet, R. A. Fisher, N. E. Phillips, D. G. Hinks, and J. D. Jorgensen, Phys. Rev. Lett. **87**, 47001 (2001).

[41] H. D. Yang, J.-Y. Lin, H. H. Li, F. H. Hsu, C. J. Liu, S.-C. Li, R.-C. Yu, and C.-Q. Jin, Phys. Rev. Lett. **87**, 167003 (2001).

[42] N. W. Ashcroft, Nature **419**, 569 (2002).

[43] M. Hanfland, K. Syassen, N. E. Christensen, and D. L. Novikov, Nature **408**, 174 (2000).

[44] T. H. Lin and K. J. Dunn, Phys. Rev. B **33**, 807 (1986).

[45] K. Shimizu, H. Ishikawa, D. Takao, T. Yagi, and K. Amaya, Nature **419**, 597 (2002).

[46] V. V. Struzhkin, M. I. Eremets, W. Gan, H.-K. Mao, and R. J. Hemley, Science **298**, 1213 (2002).

[47] S. Deemyad and J. S. Schilling, Phys. Rev. Lett. **91**, 167001 (2003).

[48] N. E. Christensen and D. L. Novikov, Phys. Rev. Lett. **86**, 1861 (2001).

[49] J. B. Neaton and N. W. Ashcroft, Nature **400**, 141 (1999).

[50] D. U. Gubser and A. W. Webb, Phys. Rev. Lett. **35**, 104 (1975).

[51] B. Sundqvist and O. Rapp, J. Phys. F: Metal Phys. **79**, L161 (1979).

[52] M. L. Cohen M. M. Dacorogna and P. K. Lam, Phys. Rev. B **34**, 4865 (1986).

[53] V. G. Vaks, M. I. Katsnelson, V. G. Koreshkov, A. I. Likhtenstein, O. E. Parfenov, V. F. Skok, V. A. Sukhoparov, A. V. Trefilov, and A. A. Chernyshov, J. Phys.: Condens. Matter **1**, 5319 (1998).

[54] G. Profeta, C. Franchini, N. N. Lathiotakis, A. Floris, A. Sanna, M. A. L. Marques, M. Lüders, S. Massidda, E. K. U. Gross, and A. Continenza, Phys. Rev. Lett. **96**, 047003 (2006).

[55] A. Sanna, C. Franchini, A. Floris, G. Profeta, N. N. Lathiotakis, M. Lüders, M. A. L. Marques, E. K. U. Gross, A. Continenza, and S. Massidda, Phys. Rev. B **73**, 144512 (2006).

[56] W. L. McMillan, Phys. Rev. **167**, 331 (1968).

[57] C. F. Richardson and N. W. Ashcroft, Phys. Rev. B **55**, 15130 (1997).

[58] A. Görling and M. Levy, Phys. Rev. A **50**, 196 (1994).